Spatiotemporal dynamics due to stick-slip friction in an elastic-membrane system

D. P. Vallette and J. P. Gollub*
Physics Department, Haverford College, Haverford, Pennsylvania 19041
and Physics Department, The University of Pennsylvania, Philadelphia, Pennsylvania 19104
(Received 21 September 1992)

Frictional stick-slip dynamics is studied experimentally in an elastic continuum by means of a stretched latex membrane in contact with a translating glass rod. In contrast to other laboratory-scale experiments, the characteristic stiffness length here is small compared to the size of the system but large compared to the spatial resolution of the measurements. The internal displacement field $u(s,t)$ is measured in detail with imaging techniques, which are shown to be more sensitive than total-force measurements. The magnitudes μ of slipping events extend over a wide range and include both small localized events and large spatially extended ones. The shape of the distribution $P(\mu)$ depends somewhat on the measurement threshold and also varies with the parameters describing the frictional interaction, which are affected by wear. The frictional force increases with velocity and an instability is due to waves of detachment. The temporal statistics of slipping events are also discussed. The experimental results are compared qualitatively to simplified models of earthquake faults.

PACS number(s): 05.45.+b, 91.30.Dk, 05.40.+j

I. INTRODUCTION

Spatially extended nonlinear systems often exhibit complex spatiotemporal dynamics [1]. Because of its possible relevance to earthquake dynamics, the phenomenon of interfacial stick-slip friction has been the focus of several recent theoretical and experimental studies. A particularly intriguing feature of earthquakes is the fact that no single scale generally dominates and the distribution of sizes (seismic moments) follows an empirical power law when averaged over many faults [2,3]. This scale-invariant feature motivated Bak, Tang, and Wiesenfeld [4] to propose that earthquake faulting is a physical realization of the concept of self-organized criticality. Systems that are self-organized exhibit fluctuations on all scales without tuning of a parameter.

Subsequently, Carlson and Langer [5] investigated numerically the question of whether power-law distributions could be a property of the very simple Burridge-Knopoff (BK) [6] model of a single fault. This discrete deterministic model is based on a one-dimensional chain of elastically coupled blocks that interact frictionally with a plane surface and are also coupled to a pulling plate by a second set of elastic elements. The model is dynamically unstable because of an assumed velocity-dependent friction law $\phi(v)$ that decreases with increasing slipping velocity. Its behavior was studied in an extensive series of numerical simulations [7–11]. Many aspects of the complex behavior of earthquakes have analogues in the model, including power-law size distributions of slipping events plus larger characteristic events that can be roughly periodic in time. The time distributions of events were also investigated in order to address the problem of earthquake prediction within the framework of a simple model. These simulations have received wide attention because they show that dynamical complexity can result from stick-slip dynamics without introducing the spatial inhomogeneities and fractal fault patterns that are characteristic of natural seismic phenomena [12].

This same model has received further attention recently. de Sousa Vieira, Vasconcelos, and Nagel [13] studied the role of the characteristic velocity in the velocity-dependent friction law. They documented a continuous transition as a function of this parameter from behavior dominated by brief stick-slip events to another regime dominated by continuous global slipping. Schmittbuhl, Vilotte, and Roux [14] studied the response of the model to changes in the system size and the loading rate. They found both chaotic motion and propagating wave solutions depending on these parameters. Many other models of slipping on faults have been proposed, including discrete cellular automata [15,16] and lattice models [17], as well as continuum elastic models aimed at more realistic descriptions of geophysical materials [18,19].

There have also been quite a few experimental studies of the dynamics of slipping. For example, Tullis and Weeks [20] have investigated the frictional properties of granite sliding on granite at high normal forces; their results can be described by a friction law which depends both on the duration of contact and on the sliding velocity. Gu and Wong [21] found that wear caused by cumulative slip led to a transition from unstable stick-slip to stable sliding in a variety of materials relevant to seismology. Their observations, including transient period doubling and other nonlinear phenomena, can be described by a one-dimensional spring-slider system with a friction law similar to that used by Tullis and Weeks. Feder and Feder [22] studied an effectively two-dimensional system of elastic elements pulled across a rough surface (carpet on sandpaper). They measured the statistics of slipping events as manifested in the total force and compared the observations to what might be expected in a self-organized critical system. These various studies have shown evidence of spatiotemporal complexity in stick-slip

processes. However, one significant missing feature has been the capability of fully resolving the dynamics as a function of *both space and time.*

In this paper, we describe an experimental study of the stick-slip dynamics of a continuous elastic medium in which the time-dependent displacement field is fully resolved. The experiment is based on the interaction of a stretched rectangular membrane with a clean cylindrical glass rod. The rod is aligned parallel to the long side of the membrane, pressed against it with an adjustable normal force, and translated slowly and precisely under computer control. An array of closely spaced parallel lines is ruled on the membrane. The time-dependent displacement and velocity fields are then measured by digital image processing. (The total applied shear force is also monitored.) The slipping events are characterized by their magnitude, the logarithm of the total integrated displacement, and also by the length of the slipping region. We observe complex dynamics, including a wide range of event sizes, and we discuss the results in the context of theoretical models. We also consider several difficulties that affect any experimental study of these phenomena: the finite sensitivity of the measurement process and the presence of spatial inhomogeneities in the surface friction of real materials.

II. EXPERIMENTAL METHODS

The critical problem in designing a suitable laboratory system for studies of stick-slip dynamics in an elastic medium is the need to generate displacements large enough for optical imaging. Most materials are simply too stiff for laboratory-scale measurements. However, a latex membrane has sufficiently small elastic constants to provide suitable displacements. We use a thin latex membrane of thickness 0.25 mm and length $L=25$ cm; its elastic shear modulus μ is approximately 5000 kdyn/cm^2, and its density ρ is 0.865 g/cm^3. The membrane is stretched uniformly between two parallel aluminum plates [curved upward at the ends as shown in Fig. 1(a) to minimize end effects]. The separation w is adjustable over the range 2–4 cm. The membrane is pressed against a long cylindrical glass rod (1.1 cm diameter) oriented parallel to the long axis of the membrane, with adjustable normal force. The rod distends it as shown in the end view of Fig. 1(b). The rod is translated smoothly at a constant speed (typically 0.155 mm/s) using a microstepping motor in order to generate stress within the membrane.

We regard the system as being nearly one dimensional, so that it can be characterized by the time-dependent displacement field $u(s,t)$ (relative to equilibrium) of points at position s along the center line. We determine this field at closely spaced points by ruling a set of 100 parallel lines 2 mm apart on the free surface of the membrane, perpendicular to its axis [Fig. 1(c)]. The positions of the midpoints of the lines are determined by image processing methods. We take advantage of the sharp change in intensity across the two edges of each line, interpolate to locate the edge positions accurately, and average the two edges to obtain the position of each line center. We are able to locate the midpoints $u_i(t)$ of the lines with a precision of approximately ± 0.025 mm and time resolution of 0.13 s. This precision is approximately a factor of 10 smaller than the pixel size of the imaging system.

The total frictional force $F(t)$ experienced by the rod can also be measured using a strain gauge. The precision of these measurements is typically about $\pm 0.5\%$. Since stick-slip dynamics is often associated with a frictional force that declines with increasing velocity, we determine the velocity dependence of the frictional force quantitatively. It is necessary to use a separate narrower cell of width $w=1$ cm and length $L=7.5$ cm for this purpose to avoid instability. We determine the friction coefficient $\mu=F/F_n$, where F is the frictional force and F_n is the normal force, by stepping the velocity from rest to a constant speed. An example of the resulting transient is shown in Fig. 2. The initial level $\mu=\mu_0$ corresponds to the steady-state *static* friction of the membrane after a previous translation in the same direction. At time A (see figure) the rod is stepped to a velocity $v=0.310$ mm/s. The force rises smoothly to a new steady-state value before the motion is stopped at time B. A systematic test over a range of applied loads and velocities shows that the steady-state friction is always greater than

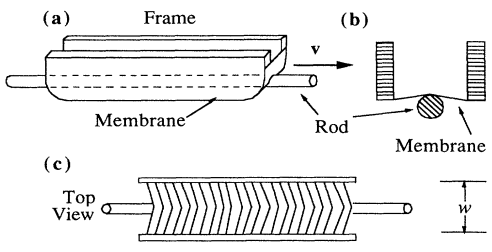

FIG. 1. Apparatus used to study stick-slip frictional dynamics of an elastic latex membrane. (a) Stretched membrane in contact with glass rod that is translated at constant speed v. (b) Side view showing distention of the membrane due to the (variable) applied normal force. (c) Top view showing lines ruled on the membrane to allow the time-dependent displacement field to be measured.

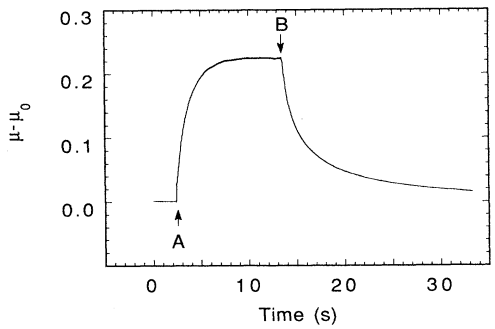

FIG. 2. Increase in the friction coefficient μ above the static value μ_0 following a step change in velocity (at time A) from $v=0$ to 0.31 mm/s. A narrow cell is used to suppress the stick-slip instability; the applied normal force is $F_n=40.5$ kdyn. The rod is stopped at B.

static friction, *and is generally an increasing function of velocity*. However, instability can occur (in a wider cell) even without velocity weakening as a consequence of waves of detachment known as Schallamach waves [23]; this phenomenon is described in Sec. III. At the positions where detachment or loss of intimate contact takes place, the frictional force is quite low and instability results.

It is possible to make a qualitative connection between the elastic properties of this experimental system and a continuum version of the BK model. In the numerical studies of Refs. [5,7–11] the relevant elastic parameter is the stiffness length ξ, which for earthquakes was suggested to be of the order of a few kilometers. We estimate the stiffness length for our system to be approximately 1 cm (see Sec. IV), which is much shorter than the system size, as it must be for a meaningful study of spatiotemporal dynamics. We also estimate the shortest slipping time as the ratio of the stiffness length to the speed $c=\sqrt{\mu/\rho}$ of shear waves. For our system $c=2500$ cm/s; therefore the slipping time (neglecting friction) is about 40 μs. Since our acquisition rate is typically 8 Hz, it is apparent that the dynamical phenomena we observe are those on longer time scales and we do not resolve the temporal structure of the fastest events.

III. EXPERIMENTAL RESULTS

A. Complex spatiotemporal dynamics

We find that the membrane system produces complex spatiotemporal dynamics. An example is shown in Fig. 3(a) for a membrane whose maximum frictional force per unit length is $f_{\max}=2.7$ kdyn/cm. (This quantity is the maximum frictional force per unit length at any time during the run, averaged over the membrane.) The solid curves are the measured displacements $u_i(t)$ (with time shown on the vertical axis) for $i=1,6,11,16,\ldots$; these points are separated initially by 10 mm when the membrane is unstressed. Half the total length of the membrane is shown. For ease in visualization we have amplified the displacements of individual curves by a factor of 20 as indicated by the scale at the top of the plot. The rod is translating to the right at speed $v=0.155$ mm/s. Several distinct types of behavior are evident in Fig. 3(a). (i) Regions of *increasing stress* appear as lines

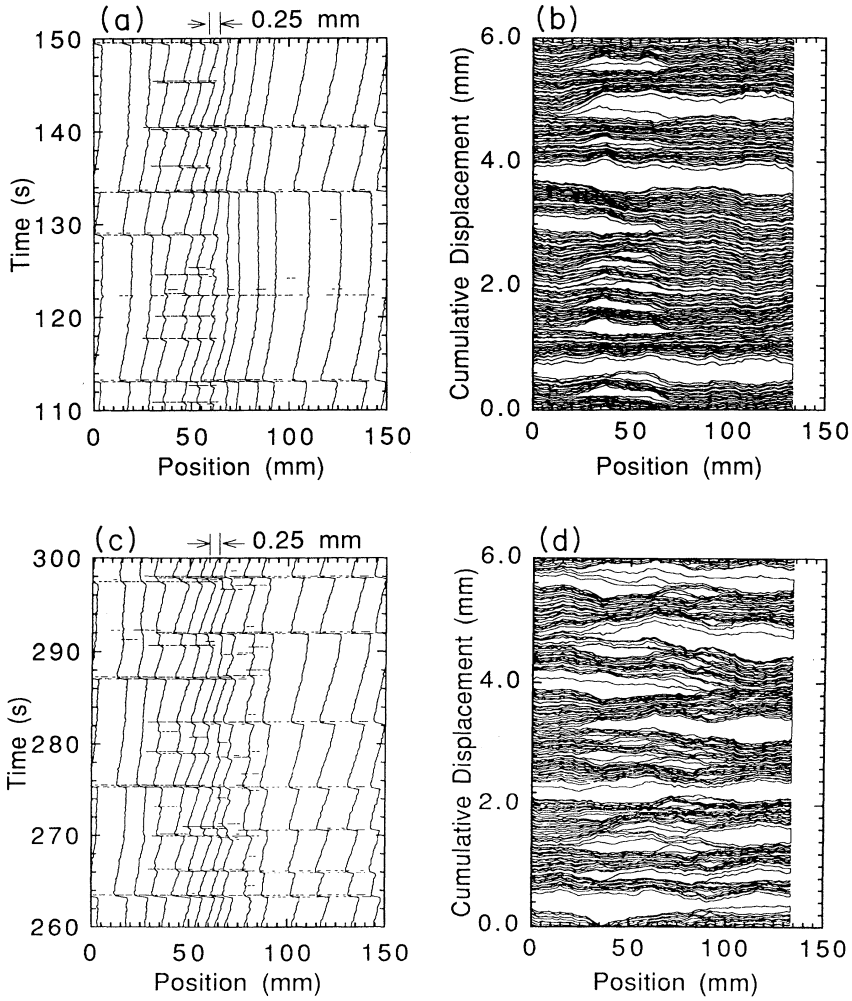

FIG. 3. (a) Displacements $u_i(t)$ of points separated initially by 10 mm (lower scale); individual displacements have been amplified by a factor of 20 (upper scale). Detected slipping events are indicated by horizontal hash marks. (b) Cumulative displacement in the rod's frame of reference. Displacements at a given time are connected by a solid line. (c) and (d) Same as (a) and (b), later in the same run. The maximum frictional force per unit length is $f_{\max}=2.72$ kdyn/cm, the width of the cell is $w=3.8$ cm, and the normal force per unit length is $f_n=396$ dyn/cm.

that are slanted slightly to the right of vertical. (ii) Sudden *large slipping events* [where $\delta u_i(t) < 0$] appear as steps at the same time for each curve $u_i(t)$. (iii) Smaller more numerous localized slipping events are also evident, especially when the diagram is magnified. In addition, one can see regions of stable creep (smooth motion of the membrane relative to the rod); these are indicated by the smooth *vertical* lines. The transient that occurs during the initial loading cycle is not shown in Fig. 3(a); the time origin is arbitrary.

Slipping events are detected by searching the digitized record [including the intervening data not shown in Fig. 3(a)], for contiguous regions of motion in space and time. The detected events during a 40-s interval are shown by horizontal hash marks in Fig. 3(a); for extended events, these appear as horizontal lines. A total of 694 events were found in the entire run of 830 s.

To eliminate most spurious events due to measurement noise, we have used a time step $\Delta t = 0.27$ s, which is larger than our minimum value, and require that the local displacement of the membrane relative to the rod exceed a threshold of 0.07 mm in this time. This choice implies a minimum average slipping speed of 0.26 mm/s for event detection. This value, which is about twice the pulling speed, excludes slow relative creep; most of the larger events are considerably faster than this. As a further precaution, we exclude events that occupy only a single point on the measured (s,t) grid. (We discuss below the effect of changing the threshold for event detection.)

The optical measurement method is quite sensitive in comparison to measurements of the total force $F(t)$; many of the localized events detected optically are too small to detect in $F(t)$. A comparison between these quantities is given in Fig. 4. The upper curve is the displacement $\hat{u}_i(t)$ for a single point on the membrane and the lower curve is the corresponding force $F(t)$. The local displacement curve reveals considerable structure that is not visible in $F(t)$.

An alternate view of stick-slip dynamics is shown in Fig. 3(b), where the cumulative displacement $\hat{u}_i(t) \equiv vt - u_i(t)$ *in the rod's frame of reference* is shown as a function of position and time. Here each curve connects all the measured points i at a given time. The large slipping events are the white regions, and the regions of sticking are the locations where there is no forward motion and several lines are superimposed. This representation shows the full spatial resolution of the data. The largest events (which move from right to left) produce a substantial fraction of the total displacement, as does the phenomenon of stable creep, indicated by regions of closely spaced parallel lines.

The stick-slip events that span only part of the system are evidently spatially inhomogeneous. Later in the same run the regions of small-scale slip have expanded to include a larger portion of the membrane, as shown in Figs. 3(c) and 3(d). These changes occur because the surface properties of the membrane evolve over time as a result of wear. The differences in surface properties between regions of creep and regions undergoing local stick-slip can also be seen from the increased slopes of the positions $u_i(t)$ in regions of stick-slip immediately following a large slipping event [Figs. 3(a) and 3(c)]. This observation suggests that the frictional force is larger in regions of stick-slip.

Though some regions may be temporarily displaced more than others from their unstressed positions, compressive stresses adjust the rates of the various processes so that over time the displacements of different parts of the membrane do not become very far out of step. Therefore the lines in Figs. 3(b) and 3(d) remain roughly horizontal.

B. Event distributions

There are many ways to characterize the dynamics statistically [2]. One is to plot the distribution of event magnitudes. We define the "moment" M by analogy to earthquake modes as *the integrated displacement over the space-time region containing the event.* [For an event lasting one time step, the moment is simply the area of the event in Figs. 3(b) and 3(d).] The *magnitude* is then defined as $\mu = \log_{10} M$. The probability distribution $P(\mu)$ is shown in Fig. 5 for the run of Fig. 3 on a semilogarithmic scale, for three different choices of the measurement threshold that is applied to discriminate against instrumental noise. (The bold line corresponds to the threshold of 0.07 mm mentioned in Sec. II A; this value is used for further analysis.) For earthquakes, this function

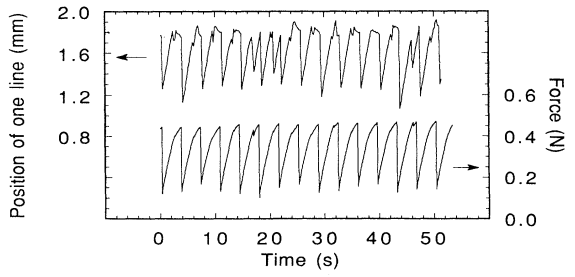

FIG. 4. Displacement $u_i(t)$ of a single point on the membrane (upper curve) and total force $F(t)$ (lower curve). The former is more sensitive to small-scale events.

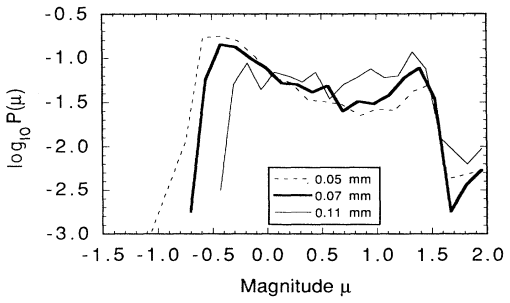

FIG. 5. Distribution $P(\mu)$ of slipping event magnitudes for the run of Fig. 3, for several choices of the measurement threshold for slip detection (see legend). A threshold of 0.07 mm (bold line) is used for further analysis.

is of the form $P(\mu)=A\exp(-b\mu)$, and the related *moment* distribution $\tilde{P}(M)$ is a power law $\sim M^{-b-1}$. Increasing the threshold eliminates some (mainly small) events; the sharp decline in $P(\mu)$ for small μ is completely determined by the choice of threshold. For the dashed case ($M=0.05$ mm), the threshold is too small, and it is clear from examining figures similar to those in Fig. 3 that measurement noise then causes separate events to be blended together, distorting the distribution. The other two cases shown in Fig. 5 have similar distributions (except at small μ). However, the statistics are not precise enough to reliably test the hypothesis of power-law behavior and the exponent of a fitted power law would depend on the choice of threshold. There is also significant variability from run to run.

Another useful way to characterize the data is to consider the *distribution of slip lengths* $P(l/w)$ as shown in Fig. 6. We normalize slip lengths l by the width w of the membrane. The sharp peak at $l/w\approx 3.5$ corresponds to events spanning our observation area, roughly half the length of the membrane. Note that (omitting the peak containing the largest events) $P(l/w)$ falls off approximately exponentially with a decay length comparable to w.

How are the *lengths* l/w of slipping events related to their *moments* M? We show this connection in Fig. 7 for each event in the run of Fig. 3. The solid line is a lower bound determined by the chosen measurement threshold of 0.07 mm (at each spatial location along the event). For events shorter than $l/w\approx 1.3$ ($l\approx 50$ mm), the smallest moments are right *at* the threshold, so we could be missing some of these events. (Recall that we have chosen a very conservative threshold to ensure that very few spurious events are detected.) Most of the detected longer events are well above the measurement threshold. This implies that the displacement at each point during slip typically increases with the length of the event. Many of the *longest* events span the entire system ($L=250$ mm). Since the measurement area is smaller than this, the moments and lengths of the longest events in the diagram are generally underestimated.

After a prolonged period of use, wear causes the maximum frictional force to rise significantly. Behavior typical when the frictional force is larger ($f_{\max}=4.7$ kdyn/cm) is shown in Fig. 8. System-wide slipping events now dominate the motion of the membrane. After each large slip the membrane adheres to the rod uniformly, as can be seen by the constant slopes of the lines in Fig. 8(a) during loading. Small-scale slips are infrequent and creep is virtually nonexistent. The absence of creep is apparent from the densely packed regions in Fig. 8(b) in which the lines do not advance along the rod, in contrast to the regular parallel pattern seen in Fig. 3(b) or 3(d). The positions of the relatively infrequent small-scale slips are not correlated.

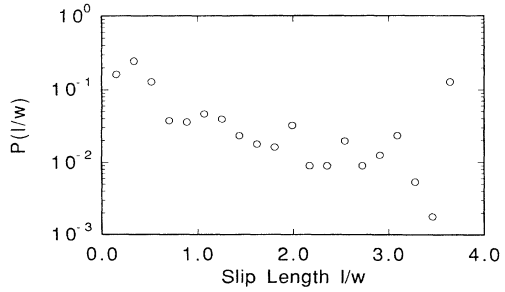

FIG. 6. Distribution $P(l/w)$ of slip lengths for the run of Fig. 3. Slips of all sizes are seen up to the size of the system. The peak in slip lengths above $l/w=3.5$ includes all slips larger than the field of view.

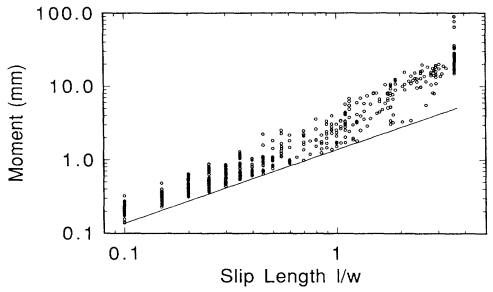

FIG. 7. Log-log plot of the moment M vs the slip length l/w. The solid line, which rises linearly with l/w, is determined by the selected measurement threshold of 0.07 mm at each measured point.

The qualitative behavior of the system varies widely with the frictional properties of the membrane, and this variability is manifested in the shape of the event magnitude distribution. Distributions for two typical runs are shown in Fig. 9. The lower curve corresponds to the run shown in Fig. 8 (larger $f_{\max}$). The peak at large magnitudes reflects the dominance of the large events. On the other hand, when $f_{\max}$ is reduced so that the smaller events are more prominent, the distribution of magnitudes is often similar to the example shown in the upper curve, which is roughly a power law with slope $b\approx 1$.

Several other parameters can be varied. For example,

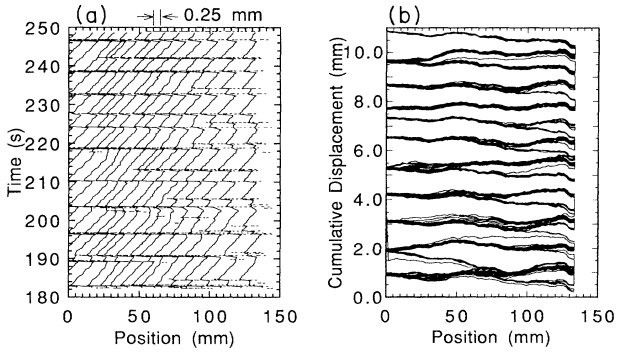

FIG. 8 (a) Displacement field $u_i(t)$ and (b) cumulative displacement field $\hat{u}_i(t)$ when the frictional force $f_{\max}$ is larger than that of Fig. 3 by a factor of 1.7. Here most of the displacement occurs in large events; small-scale slips are infrequent, and the membrane adheres to the rod most of the time. The main cause of the increased friction is wear.

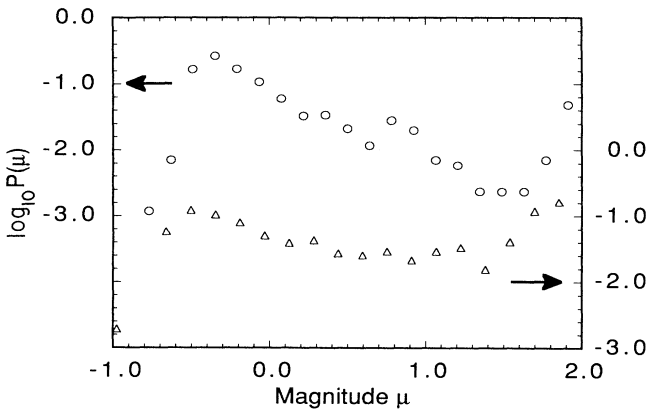

FIG. 9. Distribution $P(\mu)$ of slipping event magnitudes for two runs with different f_{max}. Vertical scales are offset as indicated by the arrows. The maximum friction for the upper curve ($f_{max}=2.5$ kdyn/cm), which has prominent small events and a slope $b \approx 1$, is about half that for the lower curve ($f_{max}=4.7$ kdyn/cm). The lower distribution is dominated by large events.

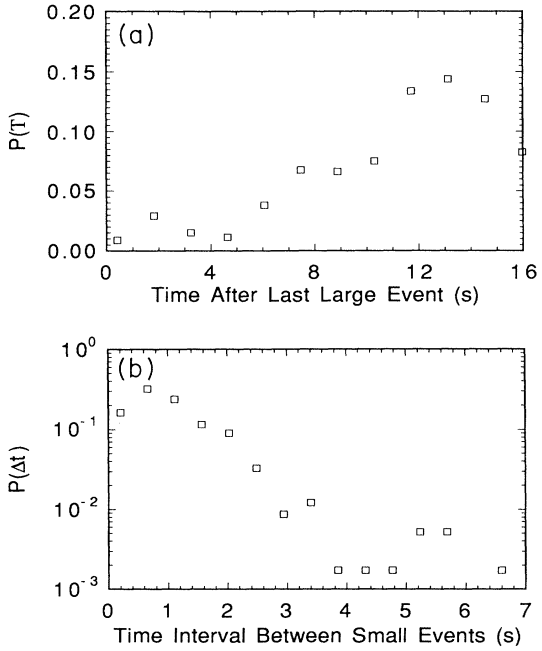

FIG. 10. (a) Distribution of times of events of any size following a large event. This drop in activity is often seen following large drops in stress. (b) Time-interval distribution between adjacent small events within a loading period. The roughly exponential falloff implies that these events are not strongly correlated in time. Data are for the run giving the upper distribution in Fig. 9.

the transverse prestretch of the membrane was approximately 5%; the behavior was not qualitatively affected by modest changes in this parameter. The results are also only weakly dependent on the normal force because the microscopic contact area does not vary strongly with pressure. However, increasing the normal force substantially (about a factor of 10 above typical values) tends to suppress the small events. Finally, the width w of the membrane is an important parameter. The instability is eliminated by reducing w substantially.

C. Temporal distributions of events

We have also investigated the temporal distribution of slipping events quantitatively for run showing a wide range of event sizes. The distribution of intervals between large events has a broad peak; this indicates approximate periodicity. The large events are usually nucleated at one end of the membrane; the reasons for this periodic nucleation at the end are unclear. Periodicity is a general property of Schallamach waves in rubber friction and is responsible, for example, for the squealing of tires during skidding.

The effects of the large events on the time distribution of small events can be seen in Fig. 10(a). Starting with a large event, the distribution of time intervals to the next event of any size often shows a gap (typically about 5 s) before rising strongly. This behavior is related to the quiescent intervals visible at times in Fig. 3(a), though Fig. 10 comes from a different run. A similar property has also been found for the BK model [10]. We would like to point out, however, that quiescence is not always observed. It is more likely to be seen in cases where the stress drop due to the major events is a large fraction of the *total* stress.

The distribution of intervals between adjacent *small* events, shown in Fig. 10(b), can be *roughly* approximated as exponential over several orders of magnitude; this would be consistent with Poisson statistics. The small events are not strongly correlated in time, though some spatial clustering is present.

D. Wear: inhomogeneity and evolution of the frictional coefficient

Ideally, the event distributions would be stationary in time and independent of spatial position. However, this situation is not easily achieved. An example of the spatial and temporal distribution of the event centers is shown in Fig. 11. It is evident both that the events tend to occur preferentially in certain regions and that there is some evolution in the predominant event locations over the course of the run. Events that span the entire observation region are not shown in this figure. These results imply that the frictional properties of the membrane vary somewhat in space and time. The spatial variations are most likely due to nonuniform wear of the material, a phenomenon that is typical for solid surfaces in contact.

This evolution due to wear is manifested in the time dependence of the steady-state frictional coefficient μ_{ss}, measured as described in Sec. II. The velocity dependence of this quantity is shown in Fig. 12. Note first that the frictional force is never lower than its static value and generally increases with the pulling speed. (Normally,

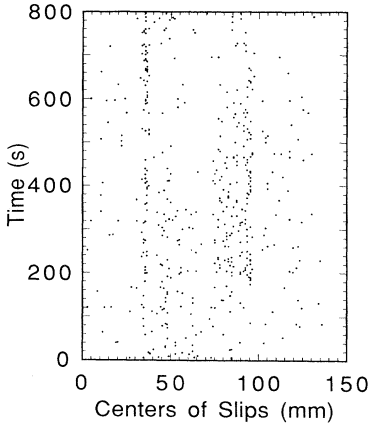

FIG. 11. Locations of identified event centers in space and time for the run of Fig. 3. Regions preferentially undergoing stick-slip motion evolve in time due to wear.

the pulling speed is 0.155 mm/s, which is in the lower part of the range shown in Fig. 12.) Second, the frictional force at a given speed v increases slowly with time over a few hours of continuous sliding, an effect that has been previously noted for rubber [24]. Finally, the curves shown in Fig. 12 can be further reduced by surface treatments such as roughening of the rod or chlorination of the membrane.

The frictional force per unit length f is not solely a function of velocity, in contrast to the simplifications made in many numerical studies. We have observed that the largest events are actually propagating waves of detachment [23]. During slipping events, the membrane loses intimate contact with the rod; this leads to a sharp decline in f which is not primarily a function of velocity. It is likely that the detachment mechanism drives even the smallest slipping events. Therefore one might regard the frictional force as having two branches; the velocity dependence is similar to that shown in Fig. 12 only when intimate contact is maintained, as for the narrow cell used to measure f without instability.

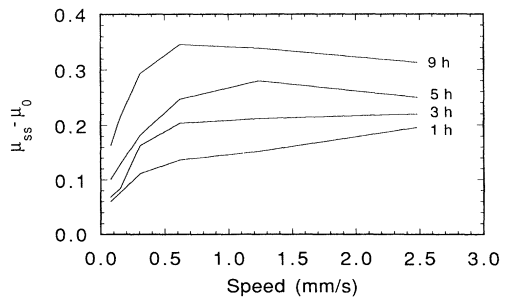

FIG. 12. Velocity dependence of the friction coefficient of latex rubber on glass, sampled after various periods of continuous moving contact. We plot the difference between the dynamic (stick-slip) and static friction coefficients, $\mu_{ss}-\mu_0$. The frictional force increases with velocity and also increases slowly with time.

IV. DISCUSSION AND CONCLUSION

We have studied the spatiotemporal dynamics of the slipping membrane system in some detail, using optical imaging methods to resolve the displacement field as a function of space and time. The spatial sensitivity is about 0.025 mm, which is small compared to all of the natural lengths in the problem. The local optical measurements are shown to be more sensitive than measurements of the total frictional force. Our central observation is that slipping events on a wide range of scales are usually found.

We have also pointed out two particular difficulties in evaluating the results. First, the smallest events are comparable to our measurement resolution. Therefore the event statistics are influenced to some extent by the choice of threshold used to discriminate against noise. However, we believe that the measured magnitude distributions are at least qualitatively correct. We do *not* generally find robust scaling behavior.

A second difficulty is that wear causes nonuniformities to develop in the frictional properties of the membrane. This nonuniformity is visible in the spatial distributions of event locations. In other cases (for example, Fig. 8), events appear to nucleate relatively homogeneously, except for the largest ones. Though the heterogeneity that is sometimes present is a nuisance, we do not believe that it is *responsible* for the observed dynamical complexity. The magnitude distribution $P(\mu)$ and other statistical properties are sensitive to the interfacial conditions, especially the maximum frictional force $f_{\max}$. The behavior may also depend on the length L of the membrane, but we have not yet resolved this issue experimentally. Length dependence is seen in some simulations [14,16].

The experiments were stimulated by numerical studies of the Burridge-Knopoff model. It is worthwhile to examine the extent to which the experimental system is analogous to the BK model. We provisionally assume that the experimental system is effectively one dimensional and consider the dynamics only on time scales long compared to that of the fundamental longitudinal mode of the membrane. A continuum equation was presented by Carlson and Langer [7] which described the essential features of the BK model. The evolution of the nondimensional displacement field $U(s,\tau)$ along the fault at position s and time τ is given by

$$\ddot{U}=\xi^2\frac{\partial^2 U}{\partial s^2}-U+\phi(2\alpha v-2\alpha\dot{U})\ , \tag{1}$$

where τ is the time, made nondimensional by a characteristic slipping time. The displacement field U is measured in units of a characteristic slipping distance. The coefficient of the second derivative is a dimensional stiffness length ξ. The velocity dependent frictional force is ϕ and v is the loading speed. The first term on the right-hand side of Eq. (1) is related to the compressional stiffness; it tends to smooth out local fluctuations in the displacement field. The linear term is a restoring force which tends to keep displacements finite. The friction law is assumed to weaken on a velocity scale α^{-1}. The model contains both scale-invariant localized events and

large delocalized events; the characteristic moment (integrated displacement) separating these two classes of events is determined roughly by the ratio ξ/α. Thus the stiffness length is an important elastic parameter.

The dynamics of the stretched membrane system may be examined by considering a small patch of membrane of width δw that is in contact with the rod. It is assumed to be uniformly compressed or extended, and to experience shear forces from the part of the membrane that is not in contact with the rod. The longitudinal strain is assumed to decrease linearly to zero at the edges of the membrane. The shear forces are determined by the shear modulus of the latex material. Since we do not treat the dynamics in the direction out of the plane of the membrane, the compressional forces acting on the patch are determined by an effective bulk modulus K_{eff} that is equal to μ. (The ordinary bulk modulus is much larger and is not relevant in a configuration where the thickness is unconstrained.) It is straightforward to show that the dynamics of the system are given by Eq. (1), but with a different frictional force. The stiffness length ξ is given by $\xi=\sqrt{w\delta w}$. Although the various approximations made in the derivation (for example, one dimensionality) are severe, it seems very unlikely that the stiffness length could be larger than w.

Our system thus contains the essential elastic properties of the BK model. However, the source of the instability is fundamentally different. As shown in Sec. III, the measured frictional force is not velocity weakening; instability is produced instead by a detachment process in which intimate contact is lost locally. The existence of stable creep is further evidence of the fact that the friction law is otherwise velocity strengthening. Therefore we do not attempt a detailed comparison between the model and the experiments.

Some of the features of the model are seen in these experiments. They include broad distributions of event sizes whose characteristics depend on the friction law, as well as large scale delocalized events that are distinct from the smaller ones. The moments of these events tend to grow faster than linearly with event length. This observation indicates that the stress drop increases with event length. The large events are nearly periodic and account for the bulk of the stress release [e.g., Fig. 8(b)]. Quiescence often occurs after these large stress drops. Some of the larger slipping events do not extend over the entire system. Therefore it is probable that we would observe a cutoff in the distribution of the largest events in a longer cell; such a cutoff is also observed in the BK model. However, the system-wide events seen in our experiments are nucleated primarily at the boundary and hence may have a different origin from the large-scale events seen in the model [9].

Our experiment is essentially one dimensional for scales larger than w, but may well be two dimensional on smaller scales. We hope eventually to study the effects of dimensionality and to utilize a circular geometry to test for end effects. Further study of the friction law would also enhance our understanding.

ACKNOWLEDGMENTS

We thank J. Carlson, C. Caroli, F. Heslot, T. Lubensky, J. Rundle, B. Shaw, and J. Socolar for helpful discussions. We thank A. E. Ruff for participating in the total-force measurements. This work was supported by NSF Grant No. 8901869.

*Electronic address: jgollub@acc.haverford.edu

[1] M. C. Cross and P. C. Hohenberg, Rev. Mod. Phys. (to be published).
[2] C. H. Scholz, *The Mechanics of Earthquakes and Faulting* (Cambridge University Press, Cambridge, 1990).
[3] Y. Y. Kagan, Nonlin. Sci. Today **2**, 1 (1992).
[4] P. Bak, C. Tang, and K. Wiesenfeld, Phys. Rev. Lett. **59**, 381 (1987).
[5] J. M. Carlson and J. S. Langer, Phys. Rev. Lett. **62**, 2632 (1989).
[6] R. Burridge and L. Knopoff, Bull. Seis. Soc. Am. **57**, 341 (1967).
[7] J. M. Carlson and J. S. Langer, Phys. Rev. A **40**, 6470 (1989).
[8] J. M. Carlson, J. Geophys. Res. **96**, 4255 (1991).
[9] J. M. Carlson, J. S. Langer, B. E. Shaw, and C. Tang, Phys. Rev. A **44**, 884 (1991).
[10] B. E Shaw, J. M. Carlson, and J. S. Langer, J. Geophys. Res. **97**, 479 (1992).
[11] J. S. Langer, B. E. Shaw, and J. M. Carlson, J. Geophys. Res. **97**, 479 (1992).
[12] Y. Y. Kagan and L. Knopoff, Geophys. J. R. Astron. Soc. **62**, 303 (1980).
[13] M. de Sousa Vieira, G. L. Vasconcelos, and S. R. Nagel (unpublished).
[14] J. Schmittbuhl, J.-P. Vilotte, and S. Roux, Europhys. Lett. (to be published).
[15] K. Chen, P. Bak, and S. P. Obukhov, Phys. Rev. A **43**, 625 (1991).
[16] J. Lomnitz-Adler, L. Knopoff, and G. Martínez-Mekler, Phys. Rev. A **45**, 2211 (1992).
[17] M. Matsuzaki and H. Takayasu, J. Geophys. Res. **96**, 19925 (1991).
[18] J. R. Rice, J. Geophys. Res. (to be published).
[19] J. B. Rundle and S. R. Brown, J. Stat. Phys. **65**, 403 (1991).
[20] T. E. Tullis and J. D. Weeks, Pure Appl. Geophys. **124**, 383 (1986).
[21] Y. Gu and T.-F. Wong, in *Nonlinear Dynamics and Predictability of Critical Geophysical Phenomena,* edited by A. Gabrielov and W. Newman (American Geophysical Union, Washington, DC, in press).
[22] J. Feder and H. J. S. Feder, Phys. Rev. Lett. **66**, 2669 (1991).
[23] A. Schallamach, Wear **17**, 301 (1971).
[24] F. P. Bowden and D. Tabor, *Friction, An Introduction to Tribology* (Doubleday, Garden City, NY, 1973).